nature methods

BRIEF COMMUNICATION

https://doi.org/10.1038/s41592-018-0183-z

Closed-loop all-optical interrogation of neural circuits in vivo

Zihui Zhang[1,2,4], Lloyd E. Russell[1,4], Adam M. Packer[1,3,4*], Oliver M. Gauld[1] and Michael Häusser[1*]

Understanding the causal relationship between neural activity and behavior requires the ability to perform rapid and targeted interventions in ongoing activity. Here we describe a closed-loop all-optical strategy for dynamically controlling neuronal activity patterns in awake mice. We rapidly tailored and delivered two-photon optogenetic stimulation based on online readout of activity using simultaneous two-photon imaging, thus enabling the manipulation of neural circuit activity 'on the fly' during behavior.

Understanding how the spatiotemporal patterns of activity in neural circuits drive behavior represents a fundamental problem in neuroscience. To define causal relationships between activity patterns and behavior we must not only measure activity patterns in identified neurons, but also make precisely targeted interventions. The ability to simultaneously read out and manipulate activity in neural circuits using an 'all-optical' combination[1] of imaging and photostimulation now allows optogenetic interventions to be targeted to individual neurons in the mammalian brain in vivo[2–7] based on their functional signature[2,4]. However, this targeting has hitherto been guided by offline analysis, which typically involves averaging activity across multiple trials. Because the activity of individual neurons can be highly variable, and their contribution to population activity can fluctuate from moment to moment[8–11], it is essential to target photostimulation guided by online measurements of activity. If readout and targeting are sufficiently rapid, this permits online closed-loop control[12] in which photostimulation is targeted to the appropriate cells and titrated to enhance and transform evolving patterns of neural activity.

Here we implemented an online feedback strategy to close the loop between optical readout (using a genetically encoded calcium indicator, GCaMP6) and optical stimulation (using an optogenetic actuator, C1V1). Our closed-loop module accesses the raw pixel data streaming in real time from the microscope, performs online analysis of population activity inferred from the calcium imaging data, and uses these results to reconfigure photostimulation rate and patterns through integrated hardware (Fig. 1a and Supplementary Fig. 1). To demonstrate the range of new experiments enabled by our flexible closed-loop approach, we used it to perform different classes of dynamic, activity-guided circuit manipulations at cellular resolution in vivo.

First, since many neural circuits are thought to use the average rate of spiking as a neural code[8,10,11,13], we implemented an all-optical 'activity clamp' in which a target activity level is maintained in individual neurons. We achieve this by tailoring photostimulation to the online readout of somatic calcium signals, which are correlated with spike rate[14]. We 'clamped' the GCaMP6 fluorescence of a neuron also expressing C1V1 in layer 2/3 of mouse neocortex at various user-defined levels through continuous on-off feedback control (Fig. 1b–d) by combining two-photon imaging and two-photon photostimulation under conditions chosen to provide sufficient signal while inducing minimal optogenetic activation (see Methods). During the closed-loop clamping period (30 s), we delivered two-photon optogenetic stimulation to the cell whenever its calcium signal fell below the target threshold (30%, 50% or 80% $\Delta F/F$). The achieved activity levels were near the target values (absolute error = 5.2 ± 4.7% $\Delta F/F$, mean ± s.d., $n = 18$ cells in six animals, Fig. 1d–f). Simultaneous cell-attached patch-clamp recordings confirmed that the clamp of the calcium signal reflected clamping of the average spike rate (after a transient instantaneous peak to reach the target; Fig. 1g and Supplementary Fig. 2). These experiments demonstrate that online feedback control can be used to tailor optogenetic stimulation to produce a specific preset level of neuronal activation. This strategy can also be applied to ensembles of neurons, efficiently mitigating the cell-to-cell and trial-to-trial variability in optogenetic responses across a neuronal population (Supplementary Fig. 3).

Next, we applied our closed-loop feedback control to manipulate sensory responses in the awake mouse (Fig. 1h). In layer 2/3 of rodent somatosensory cortex, the reliability and amplitude of sensory-evoked responses to passive whisker deflections depend on deflection amplitude[15]. We deflected single or multiple whiskers under two conditions: one evoked small amplitude (weak), and the other large amplitude (strong) neural responses (Fig. 1i,j). We used closed-loop optogenetic control to selectively boost the responses of an identified neuron to the weak sensory stimulus only when the whisker stimulus did not produce a large response (evoked activity <30% $\Delta F/F$): neuronal responses to the weak sensory stimuli were boosted to a similar level as those evoked by strong sensory stimuli (Fig. 1k,l); the manipulation also restored the reliability of trial-to-trial responses (Fig. 1m). The boosted transients in the closed-loop trials are significantly larger than the linear sum of the weak transients and the replayed photostimuli (Supplementary Fig. 4). The latencies of the boosted responses were comparable to those of strong sensory stimulation (Fig. 1n). These experiments demonstrate that we can rapidly enhance ongoing patterns of sensory-evoked activity in individual neurons in the awake mouse.

Because the spatial and temporal patterns of activity in neural circuits are crucial elements of neural codes[9,13,16], we next developed a strategy for flexibly manipulating activity of neurons based on online readout of activity patterns in the circuit. We selectively activated groups of 'target' neurons according to readout of ongoing activity in a 'trigger' neuron in layer 2/3 of mouse neocortex (Fig. 2a,b). When the activity of the trigger neuron exceeded a dynamic threshold (see Methods; Supplementary Fig. 5), we

[1]Wolfson Institute for Biomedical Research, University College London, London, UK. [2]Department of Electronic & Electrical Engineering, University College London, London, UK. [3]Present address: Oxford University, Oxford, UK. [4]These authors contributed equally: Z. Zhang, L. E. Russell, A. M. Packer.
*e-mail: adampacker@gmail.com; m.hausser@ucl.ac.uk

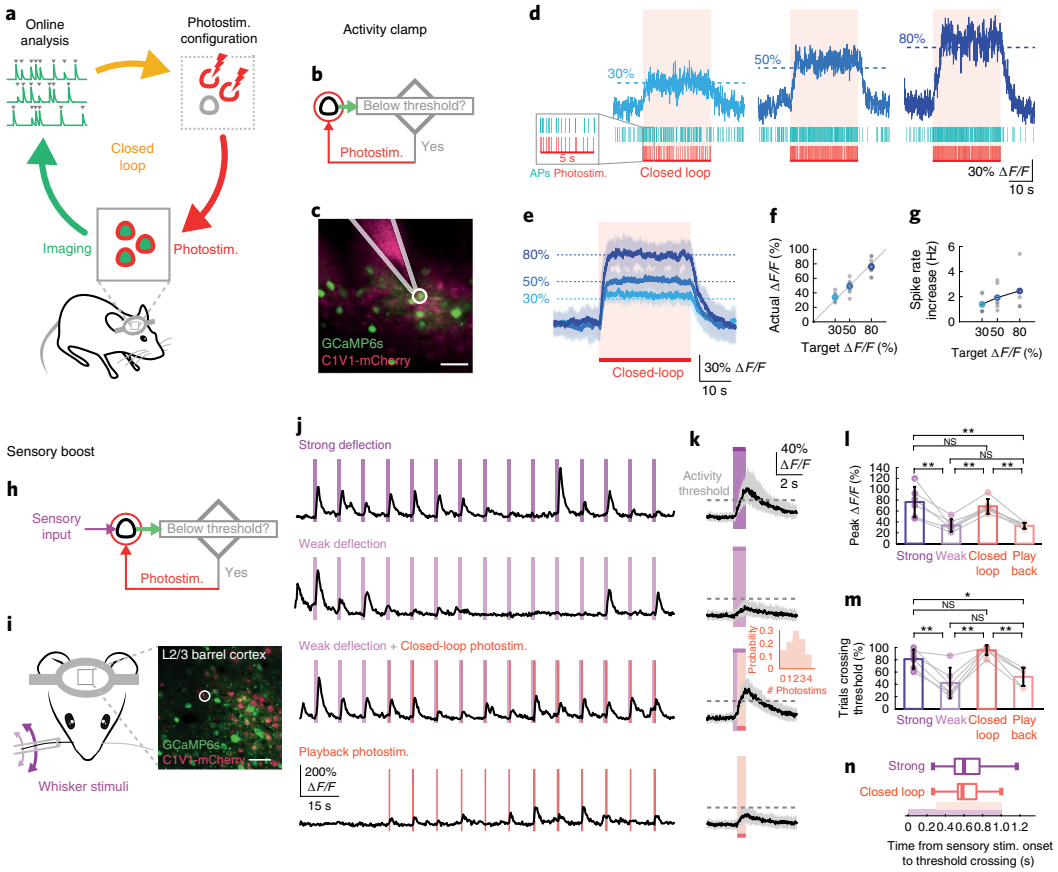

Fig. 1 | Targeted closed-loop all-optical readout and control in vivo. a, Schematic of the closed-loop all-optical control system in which two-photon imaging is combined with simultaneous two-photon photostimulation (photostim.). **b**, Experimental strategy for the activity clamp paradigm. **c**, Simultaneous cell-attached recording from a neuron (white circle) that was under activity clamp in layer 2/3 of mouse somatosensory cortex expressing GCaMP6s and C1V1. Alexa 594 was put in the pipette for visualization. Scale bar, 50 µm. **d**, Top, calcium transient from a single neuron clamped at three different activity levels (30%, 50% and 80% $\Delta F/F$; 30 s clamping period). Middle, raster plot of electrophysiologically recorded action potentials (APs) from the neuron in **c** during single trials. Bottom, photostimulation times. **e**, Mean activity clamp (30 s clamp period) of 18 cells in somatosensory and visual cortex of awake animals. Shaded area is s.d. Same photostimulation parameters as in **d**. $n = 18$ cells in six animals. **f**, Calcium signal levels achieved during activity clamp in **e** versus target calcium signal levels. Gray points are individual cells, colored points are average. **g**, Spike rate increase during activity clamp at three different target calcium signal levels, measured by simultaneous electrophysiological recording ($n = 7$ cells in five mice under anesthesia). **h**, Experimental strategy for closed-loop boosting of sensory responses. **i**, Left, configuration of whisker stimulation and two-photon imaging. Right, field of view in the C2 barrel of mouse somatosensory cortex. A neuron that responded to single whisker deflections was selected as the target (white circle). Scale bar, 50 µm. **j**, Calcium transients from the target neuron in **i** recorded while the mouse was presented with a train of single whisker deflections (purple). Top row, response to strong whisker deflections. Second row, response to weak whisker stimuli. Third row, neural responses to weak whisker deflection were boosted by photostimulation (red) if the activity recorded online was below a predefined threshold after 300 ms from the onset of the whisker deflection until the end of the deflection. Bottom row, playback photostimuli in closed-loop trials. **k**, Calcium transients during individual sensory stimulation trials (black traces are the median value of all trials; gray shaded areas show the interquartile ranges (25–75% quantiles); $n = 6$ neurons in four animals). Top, calcium signal during a strong sensory stimulus. Second from top, responses to weak sensory stimuli. Third from top, photostimulation boosted the calcium signal to pass activity threshold (30% $\Delta F/F$) response during closed-loop intervention (inset shows the number of photostimuli delivered in each trial). Bottom, response to photostimulation alone. Purple, 1 s whisker stimulation; red, closed-loop intervention. **l**, Comparison of peak neural response (mean ± s.d.) to different types of stimuli (strong, weak, closed-loop and playback. $P = 0.00014$, one-way analysis of variance (ANOVA), $^{**}P = 0.0013$, strong (76.5 ± 27.9% ΔF/F) versus weak (33.5 ± 11.5% ΔF/F); $^{**}P = 0.0011$, weak versus closed loop (68.6 ± 13.5% ΔF/F); $^{**}P = 0.007$, closed loop versus playback (32.8 ± 5.3% ΔF/F); not significant (NS) $P = 0.84$, strong versus closed loop; NS $P = 0.99$, weak versus playback; $^{**}P = 0.0011$, strong versus playback; $n = 6$ cells in four animals). **m**, Robustness of the neuronal response to different stimuli across trials with Δ F/F response to stimulation > 30%. ($P = 0.00006$, one-way ANOVA, $^{**}P = 0.0037$, strong (81.1 ± 15.4%) versus weak (42.2 ± 24.7%); $^{**}P = 0.0001$, weak versus closed loop (95.6 ± 8.1%); $^{**}P = 0.0013$, closed-loop versus playback (52.2 ± 14.9%); NS $P = 0.47$, strong versus closed loop; NS $P = 0.74$, weak versus playback; $^{*}P = 0.036$, strong versus playback; $n = 6$ cells in four animals.) Data are presented as mean ± s.d. **n**, Time taken for sensory-evoked responses to cross the 30% $\Delta F/F$ threshold for strong sensory-evoked responses (top values, interquartile range, 500–767 ms) and weak sensory-evoked responses boosted by photostimulation (bottom values, interquartile range, 533–733 ms) is similar ($P = 0.33$, Wilcoxon signed-rank test (two-sided), $n = 90$ trials, 6 cells in four animals). Purple bar, whisker stimulation window (1 s); red, photostimulation window (starting 300 ms after the onset of whisker stimulation). Data are presented as box-and-whisker plots displaying median, interquartile and 90% ranges.

rapidly (Supplementary Fig. 6) activated the target neuron ensemble (Fig. 2c,d). During this closed-loop protocol, the activity of the trigger neuron and the associated target neurons became highly correlated (Supplementary Fig. 7a). Next, we multiplexed the approach using multiple feedback loops running concurrently, enabling independent multicell readout combined with control

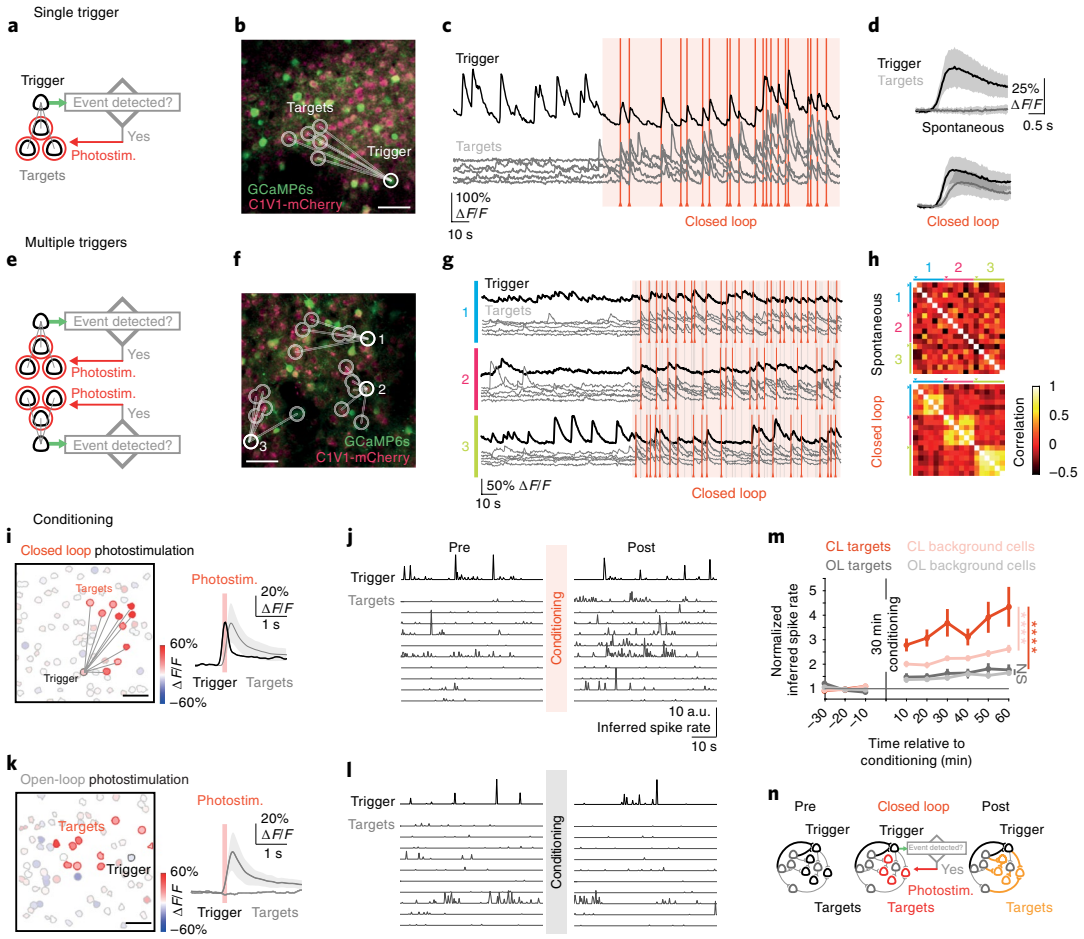

Fig. 2 | Online activity-guided photostimulation of neuronal ensembles can induce long-term plasticity of network activity. a, Experimental strategy for dynamic interrogation of ensembles with a single trigger neuron and multiple targets. **b**, Field of view in layer 2/3 of mouse somatosensory cortex coexpressing GCaMP6s and C1V1 in an awake mouse. A trigger neuron (thick white circle) was selected to drive photostimulation of five target neurons (thin white circles; representative example of six independent experiments with similar results). **c**, Calcium signal recorded from trigger neuron (top) and target neurons (bottom). Target neurons are photostimulated (red vertical lines) upon detection of an event in trigger neuron during closed-loop control period (140 s, shaded area). **d**, Calcium transients (mean ± s.d.) averaged across detected events during spontaneous activity period (top) and closed-loop control period (bottom) ($n = 6$ trigger neurons, black trace; each trigger neuron was associated with a different group of five target neurons; gray trace). **e**, Experimental strategy for dynamic interrogation of ensembles with multiple trigger neurons and multiple targets. **f**, Field of view in layer 2/3 of mouse somatosensory cortex in an awake mouse. Three trigger neurons (numbered) were selected to drive photostimulation of three different groups of five target neurons (indicated by lines from triggers to targets; representative example from three independent experiments with similar results). **g**, Calcium transients in which target neurons (gray traces) were photostimulated (red vertical lines; gray vertical lines show when other target group(s) was stimulated) when their corresponding trigger neurons crossed an activity threshold (black traces). **h**, Pearson's correlation matrices of calcium transients recorded from trigger and target neurons in **g**, during spontaneous period (top) and closed-loop period (bottom). Each color bar covers rows (or columns) corresponding to neurons in the same trigger-targets group, with arrows indicating trigger neurons. **i**, Closed-loop conditioning. Ten target cells (red contours) were activated when an event was detected in a trigger cell (black contour) in layer 2/3 of somatosensory cortex in an awake mouse. Left, spatial map of all detected neurons in field of view. Color shows amplitude of each neuron's calcium transients averaged in a 500 ms window after onset of photostimulation. Right, average calcium transient of trigger cell (black) and target cells (gray) after photostimulation (red vertical line; center value is mean; shaded area shows s.d.). **j**, Example spike rate inferred from calcium imaging of trigger cell (top row) and target cells (bottom rows) before and after closed-loop photostimulation (30 min conditioning in each experiment; a.u., arbitrary units). **k**, Same as **i**, but for open-loop photostimulation. **l**, Same as **j** but for open-loop photostimulation. **m**, Inferred spike rate of target cells increased significantly after closed-loop (CL) photostimulation (red, $^{****}P = 1.3 \times 10^{-10}$, Wilcoxon signed-rank test (two-sided), $n = 57$ cells in six animals) but not in open-loop (OL) photostimulation targets (gray, NS $P = 0.11$, Wilcoxon signed-rank test (two-sided), $n = 56$ cells in six animals). Change in inferred spike rate after closed-loop photostimulation was significantly higher than change after open-loop photostimulation ($^{****}P = 3.5 \times 10^{-8}$, Wilcoxon rank sum test (two-sided); values are mean ± s.e.m.; all statistical tests in panel were performed on average inferred spike rates of whole pre- or post-conditioning recording). **n**, Schematic showing potential loci of plasticity. Closed-loop photostimulation may have induced changes in connections from upstream neurons driving trigger and target neurons to the target neurons, direct and indirect connections from trigger to target neurons, and connections between the targets themselves, in addition to possible changes in intrinsic excitability (yellow). Scale bars in **b**, **f**, **i** and **k** are 50 µm.

of multiple ensembles. We selected multiple trigger neurons in a single field of view, each with a different corresponding set of targets (Fig. 2e,f), and the target neuron groups were selectively activated when the activity of the appropriate trigger neuron exceeded its threshold (Fig. 2g). Activity across the trigger and relevant target neurons again became highly correlated during this closed-loop protocol (Fig. 2h and Supplementary Fig. 7b). These experiments demonstrate that we can use our closed-loop strategy to flexibly manipulate the temporal and spatial pattern of neural circuit activity.

The ability to activate ensembles of neurons based on rapid detection of activity patterns in defined trigger neurons allows us to 'yoke together' the activity of user-defined neuronal ensembles. Such correlated activity is the mechanistic hallmark of many theories of synaptic plasticity, which are challenging to test directly in the intact brain[17–19].To drive plasticity mechanisms in a targeted manner, we used our closed-loop strategy to repeatedly drive activity in an ensemble of target neurons based on activity in a trigger neuron, and then monitored the resulting changes in activity in the local network after this conditioning period (Fig. 2i,j). We compared these results with changes resulting from activation of a similar number of target neurons using an 'open-loop' protocol, which avoids yoking together the activity of an ensemble with that of a trigger cell (Fig. 2k,l). After the closed-loop conditioning period, there was a persistent and significant increase in the spontaneous activity of the target neurons ($P<0.0001$, Wilcoxon signed-rank test (two-sided), $n=57$ cells in six animals, Fig. 2m, see also Supplementary Figs. 8 and 9), which continued to increase post-conditioning. The changes were more pronounced than in the open-loop protocol, despite the photostimulation-triggered activity in the target cells and number of stimuli being similar (Supplementary Fig. 10a–c). The spontaneous activity of background cells was also enhanced, though to a lesser extent than in the target cells (Supplementary Fig. 11). The inferred spike rate of the target cells became larger after conditioning, especially in episodes following detected events in the trigger cell (Supplementary Fig. 12a), indicating long-lasting changes in the temporal synchrony of our artificial ensemble. These findings suggest that optically yoking together the activity of a trigger neuron with a neighboring ensemble can lead to specific and durable reconfiguration of the functional connectivity patterns in the network. This is likely to involve changes at multiple loci in the network (Fig. 2n), including upstream and downstream connections and changes in intrinsic excitability[20]. Further work is required to examine the nature and relative importance of these changes in the network. These results indicate that our all-optical closed-loop strategy can be used to probe the mechanisms and function of plasticity induced by manipulating correlated activity with cellular resolution in neural circuits of awake animals.

The applications described above show that our all-optical closed-loop interrogation strategy allows flexible manipulation of neural circuits guided by ongoing activity. Previous approaches to closed-loop control of neural activity[21–24], based on electrophysiological readout and stimulation, or a combination of electrophysiological readout and optogenetic stimulation, lacked either the ability to read out activity from genetically and anatomically targeted neurons, or the ability to target photostimulation to particular neurons. Our approach solves these problems by harnessing the spatial precision of two-photon imaging and two-photon photostimulation to enable flexible targeting of readout and manipulation to visualized neurons. Our strategy could in principle be implemented using a range of genetically encoded sensors and optogenetic probes, enabling multiplexed imaging and control of different populations by selective expression of different sensors and actuators. Enhancing the speed of the online feedback loop using future generations of genetically encoded calcium or voltage sensors and optogenetic probes with faster kinetics would further extend the reach of this approach. Closed-loop all-optical control enables new experiments in which the temporal and rate codes of neural circuits can be manipulated in a targeted manner as they evolve during behavior. This allows direct tests of models of circuit connectivity, dynamics and plasticity through on-the-fly manipulation of activity patterns. It could also be used to correct aberrant activity patterns in disease conditions such as epilepsy[21,22] and Alzheimer's disease[25], and could provide the basis of a new generation of optical brain-machine interfaces.

Online content

Any methods, additional references, Nature Research reporting summaries, source data, statements of data availability and associated accession codes are available at https://doi.org/10.1038/s41592-018-0183-z.

Received: 18 July 2017; Accepted: 4 September 2018;
Published online: 12 November 2018

References

1. Emiliani, V., Cohen, A. E., Deisseroth, K. & Häusser, M. *J. Neurosci.* **35**, 13917–13926 (2015).
2. Rickgauer, J. P., Deisseroth, K. & Tank, D. W. *Nat. Neurosci.* **17**, 1816–1824 (2014).
3. Szabo, V., Ventalon, C., De Sars, V., Bradley, J. & Emiliani, V. *Neuron* **84**, 1157–1169 (2014).
4. Packer, A. M., Russell, L. E., Dalgleish, H. W. & Häusser, M. *Nat. Methods* **12**, 140–146 (2015).
5. Forli, A. et al. *Cell Rep.* **22**, 3087–3098 (2018).
6. Mardinly, A. R. et al. *Nat. Neurosci.* **21**, 881–893 (2018).
7. Yang, W., Carrillo-Reid, L., Bando, Y., Peterka, D. S. & Yuste, R. *eLife* **7**, e32671 (2018).
8. Shadlen, M. N. & Newsome, W. T. *Curr. Opin. Neurobiol.* **4**, 569–579 (1994).
9. Rieke, F. *Spikes: Exploring the Neural Code*. (MIT Press, Cambridge, MA, 1999).
10. Pouget, A., Dayan, P. & Zemel, R. *Nat. Rev. Neurosci.* **1**, 125–132 (2000).
11. Averbeck, B. B., Latham, P. E. & Pouget, A. *Nat. Rev. Neurosci.* **7**, 358–366 (2006).
12. Grosenick, L., Marshel, J. H. & Deisseroth, K. *Neuron* **86**, 106–139 (2015).
13. deCharms, R. C. & Zador, A. *Annu. Rev. Neurosci.* **23**, 613–647 (2000).
14. Helmchen, F., Imoto, K. & Sakmann, B. *Biophys. J.* **70**, 1069–1081 (1996).
15. Simons, D. J. *J. Neurophysiol.* **41**, 798–820 (1978).
16. Bruno, R. M. *Curr. Opin. Neurobiol.* **21**, 701–708 (2011).
17. Hebb, D. O. *The Organization of Behavior*. (Wiley, New York, 1949).
18. Martin, S. J., Grimwood, P. D. & Morris, R. G. *Annu. Rev. Neurosci.* **23**, 649–711 (2000).
19. Carrillo-Reid, L., Yang, W., Bando, Y., Peterka, D. S. & Yuste, R. *Science* **353**, 691–694 (2016).
20. Zhang, W. & Linden, D. J. *Nat. Rev. Neurosci.* **4**, 885–900 (2003).
21. Paz, J. T. et al. *Nat. Neurosci.* **16**, 64–70 (2013).
22. Krook-Magnuson, E., Armstrong, C., Oijala, M. & Soltesz, I. *Nat. Commun.* **4**, 1376 (2013).
23. Newman, J. P. et al. *eLife* **4**, e07192 (2015).
24. Prsa, M., Galiñanes, G. L. & Huber, D. *Neuron* **93**, 929–939 (2017).
25. Iaccarino, H. F. et al. *Nature* **540**, 230–235 (2016).

Acknowledgements

We thank I. Bianco, H.W. Dalgleish, M. Fisek, B. Judkewitz, P. Latham, D. Selviah and A. Roth for helpful discussions and comments on the manuscript; K. Deisseroth (Stanford University) for access to AAVdj virus; and Bruker Corporation for software support. We thank D. Selviah for support and training of Z.Z. This work was supported by grants from the Wellcome Trust, EMBO, ERC (AdG 695709) and the BBSRC (BB/N009835) to M.H. Z.Z. was supported by the Faculty of Engineering at University College London. L.E.R. was supported by the Medical Research Council (MRC). O.M.G. was supported by the Wellcome Trust and MRC. A.M.P. was supported by the European Commission (Marie Curie International Incoming Fellowship grant no. 328048).

Author contributions

Z.Z. and L.E.R. developed the closed-loop software. Z.Z. performed all-optical experiments and analyzed data. O.M.G., L.E.R. and A.M.P. performed animal surgeries. A.M.P. performed cell-attached recordings. O.M.G. prepared the sensory stimulation setup. L.E.R., A.M.P. and M.H. conceived the project. Z.Z., L.E.R., A.M.P. and O.M.G. designed detailed experimental protocols. Z.Z., L.E.R., A.M.P. and M.H. wrote the paper. All authors discussed the results and contributed to revision of the manuscript.

Competing interests

The authors declare no competing interests.

Additional information

Supplementary information is available for this paper at https://doi.org/10.1038/s41592-018-0183-z.

Reprints and permissions information is available at www.nature.com/reprints.

Correspondence and requests for materials should be addressed to A.M.P. or M.H.

Publisher's note: Springer Nature remains neutral with regard to jurisdictional claims in published maps and institutional affiliations.

Methods

Virus injections. All experimental procedures were carried out under license from the UK Home Office in accordance with the UK Animals (Scientific Procedures) Act (1986). Surgeries were performed as described previously[4]. Female adult mice (about 4–8 weeks old) were anesthetized with isoflurane (5% induction, 1.5% maintenance). A craniotomy was made above barrel cortex or visual cortex and 1 µl of a mixture of AAVdj-CaMKIIa-C1V1(E162T)-TS-P2A-mCherry-WPRE (Stanford Neuroscience Gene Vector and Virus Core, genomic titer, 7.22×10^{12}) and AAV1-hSyn-GCaMP6s-WPRE-SV40 (Penn Vector Core, genomic titer, $2.04–3.25\times10^{13}$) or AAV1-hSyn-GCaMP6f-WPRE-SV40 (Penn Vector Core, genomic titer, 3.45×10^{13}) virus (dilution factor 10:1) was injected into layer 2/3 (~300 µm deep)[4]. In most experiments (Figs. 1 and 2a–h), GCaMP6s was chosen for its higher reliability in reporting spikes[26] (Supplementary Fig. 13a) to optimize the accuracy of online and offline analysis. For the plasticity experiments in Fig. 2i–n, we used the faster and lower-affinity GCaMP6f to maximize the speed of the feedback loop and minimize any disruption of calcium buffering. For chronic imaging, a metal headplate with a 5 mm circular imaging well was fixed to the skull with dental cement (Super-Bond C&B, Sun-Medical) before virus injection before we performed a larger craniotomy and installed a glass coverslip 'window.'

Imaging and photostimulation. Simultaneous all-optical imaging and photostimulation[2–7,27–35] was performed using a custom in vivo dual-beam path microscope (Ultima, Bruker Corporation). Two-photon imaging (512×512 pixel resolution per frame, 30 frames per second) of layer 2/3 mouse cortex (about 100–300 µm deep) was performed by resonant-galvanometer raster scanning a femtosecond-pulsed laser beam (Chameleon Ultra II, Coherent). A ×25 objective with numerical aperture (NA) of 0.95 (Leica) was used for all experiments. GCaMP6s (or GCaMP6f) was imaged with excitation wavelength of 920 nm and mCherry was imaged at 765 nm (field-of-view size, 268×268 µm; frame rate, 30 Hz; power on sample, 30 to 50 mW; Chameleon laser). These imaging parameters were chosen to be similar to those that have been used for imaging GCaMP6 signals in layer 2/3 in vivo with sufficient imaging quality[4,7,26,36], and to minimize imaging 'cross-talk,' that is, activation of C1V1 with the imaging laser[2,4,7] (Supplementary Table 1). To experimentally optimize the imaging parameters, we previously performed two-photon imaging of a neuron with simultaneous electrophysiological recording[26] and increased the power and/or dwell time per neuron to determine when imaging evoked spikes[4] (see also refs. [5–7,37]). We then chose imaging conditions that gave sufficient imaging quality while not inducing a significant change in the spike rate. Imaging at a higher power or lower scanning speed and/or using a smaller field of view could lead to photoactivation[4–7,37]. Therefore, imaging power needs to be carefully assessed for each experimental configuration, as the optimum parameters and thus the tradeoff between imaging quality and cross-talk are expected to depend on expression levels, kinetics and sensitivities of the opsin and the activity sensor, field of view size and imaging dwell times. The excitation source for spiral-scanning photostimulation (15–20 µm in diameter, covering the targeted cell body)[4,7,19,38] was a femtosecond-pulsed laser fixed at 1,070 nm (Fidelity, Coherent; average output, 2 W; pulse width, 55 fs; repetition rate, 70 ± 2 MHz; seven experiments in Fig. 1c–g (10–20 ms duration, 30 mW on sample), nine experiments in Fig. 2a–h (5×10 ms spirals at 100 Hz, 30 mW per cell) and six experiments in Fig. 2i–m (12–25×10 ms spirals at 100 Hz; 30 mW per cell)), or fixed at 1,030 nm (Satsuma HP2, Amplitude Systèmes; average output, 20 W; pulse width, 280 fs; repetition rate, 2 MHz; 11 experiments in Fig. 1e–g (10–20 ms duration, 10 mW on sample), six experiments in Fig. 1h–n (50–80 ms duration, 6–12 mW on sample), eight experiments in Supplementary Fig. 3 (30 ms duration, 6–12 mW per cell) and six experiments in Fig. 2i–m (15×10 ms spirals at 100 Hz, 4 mW per cell)). The plasticity protocol did not lead to changes in nuclear fluorescence or the activity level triggered by photostimulation across days (Supplementary Fig. 14). A reflective multilevel spatial light modulator (SLM; OverDrive Plus SLM, Meadowlark Optics/Boulder Nonlinear Systems; 7.68×7.68 mm active area, 512×512 pixels, optimized for 1,064 nm) was coupled to the microscope, with its active area relayed to the back aperture of the objective as described[4]. The weighted Gerchberg-Saxton algorithm[39] was used to calculate holograms to be displayed on the SLM. The weights were adjusted to compensate for the difference in diffraction efficiency between holographic spots. The maximum number of neurons that can be photostimulated simultaneously is mainly limited by the laser power. Although here we demonstrated stimulation of groups of about ten neurons, given sufficient laser power, the method can be extended to applications in which addressing more neurons (>100) is desired. The closed-loop approach could in principle be combined with other photostimulation strategies such as temporal focusing[2,40–47]. The spatial resolution of photostimulation can be further improved using the somatic targeting opsins that are currently under active development in the field[5,6,48,49]. All experiments were performed in awake mice except those with electrophysiological recordings in Fig. 1g and Supplementary Fig. 2, where the animals were anesthetized.

Online analysis and closed-loop stimulation control. Raw data from the imaging acquisition card was made available to our custom closed-loop interface (Supplementary Fig. 1a,b) written in .NET Framework (Microsoft Visual Basic) using the PrairieLink application programming interface, which allows communication between external, custom-written software and standard microscope control software (Prairie View, Bruker Corporation). The raw data consisted of a continuous stream of intensity samples and required interpretation using knowledge of the following acquisition parameters: samples per pixel, pixels per line, lines per frame, acquisition bit depth and bidirectional scan pattern. When online motion correction was enabled (used in Fig. 1i–n and Supplementary Fig. 3) to correct lateral shifts in the field of view (Supplementary Fig. 15), the raw data was converted into 512×512 frames and then registered to a preloaded reference image using a discrete Fourier transform–based algorithm[50]. The data conversion and motion correction process was accelerated using a graphics processing unit (NVIDIA GeForce GTX 750 Ti). The average signal from each predefined region of interest was extracted from the data stream, and then normalized by either the average value during spontaneous activity or the 60 frames before sensory stimulation was delivered. The frames recorded during photostimulation were not used for online decision making and were interpolated in offline processing. The activity threshold used for event detection in the trigger cells in Fig. 2 was continuously updated to be the mean + 2 s.d. and mean + 3 s.d. of the previous 60 frames (2 s), respectively. A higher threshold was used in the closed-loop plasticity protocol such that photostimulation of the target cells was paired with large burst-like events in the trigger cell (the $\Delta F/F$ threshold of photostimulation is 39 ± 4.4%, mean ± s.e.m.). More active cells were selected to be the trigger cells to obtain a large number of trials during the pairing period. (In the closed-loop experiments, the baseline activity levels of the trigger cells were > 93.1 ± 4.0% of the other cells detected in the fields of view; in the open-loop experiments, the baseline activity levels of the trigger cells were 90.8 ± 4.0% of the other cells detected in the fields of view; $P=0.51$, Wilcoxon rank sum test (two-sided).) In the open-loop experiment in Fig. 2, photostimulation was disabled in a 500 ms window after an event was detected in the trigger cell to avoid pairing between the trigger and target cells. Each plasticity experiment consisted of 30-min imaging of spontaneous activity followed by 30-min photostimulation conditioning and 60-min recording of spontaneous activity. Custom SLM control software (Supplementary Fig. 1d) using the Blink software development kit (Meadowlark Optics) written in C++ (Microsoft Visual Studio 2013) was used to load the precomputed phase masks that could generate different combinations of the beamlets targeting the predefined target-neuron groups into the SLM controller's buffer before the start of the experiment. When an online decision of the photostimulation pattern was made, the index of the required phase mask was sent from the closed-loop interface to the SLM control software via transmission control protocol (TCP) communication (Supplementary Note 1), and the required hologram (if different from the current one) was displayed on the SLM via the SLM driver electronics (Meadowlark Optics/Boulder Nonlinear Systems). Spiral stimulation (driven by Prairie View) was triggered by sending short voltage pulses (10–20 ms, 5 volts) to the microscope control electronics via an analog output device (USB-6212, National Instruments). For sensory stimulation the closed-loop interface sent a command via TCP to custom software written in MATLAB (2016a, MathWorks) which then output one of multiple different waveforms via an analog-output device (USB-6343, National Instruments) to control a piezoelectric actuator for whisker stimulation.

Sensory stimulation. For single-whisker stimulation, C2 whisker was inserted into a glass capillary attached to a one-dimensional piezoelectric actuator (PL127.11, Physik Instrumente). For multiwhisker stimulation, whiskers were deflected using a star-shaped paddle attached to a two-dimensional piezoelectric actuator (NAC2710-A01, Noliac). Weak and strong whisker stimuli were delivered by driving the piezoelectric actuator with sinusoidal waveforms (20 Hz, 1-s duration once every 10 s) of two different amplitudes (1.5–4 V for strong deflections and 0.5–2 V for weak deflections; the amplitude was adjusted based on the response of the target cell to produce significant differences in response reliability; Fig. 1m). During whisker stimulation, head-fixed animals were awake, sitting in a tube. Barrels were located by combining whisker stimulation with widefield fluorescence imaging using one-photon blue excitation provided by a light-emitting diode (Thorlabs) together with a ×5, 0.1 NA air objective (Olympus) and a complementary metal-oxide semiconductor camera (ORCA-Flash4.0, Hamamatsu; approximate field of view 1.5 mm×1.5 mm; 512×512 pixel resolution, 10 frames per second).

Electrophysiological recording. For electrophysiological validation of activity clamp experiments, acute craniotomies were performed ~3 weeks after virus injection and two-photon targeted patch-clamp recordings[51,52] were made using glass pipettes pulled from borosilicate glass (~5 MΩ pipette resistance) and filled with artificial cerebrospinal fluid (150 mM NaCl, 2.5 mM KCl, 10 mM HEPES, 1.5 or 2 mM $CaCl_2$ and 1 mM $MgCl_2$). Alexa Fluor 594 (20 µM) was included in the pipette solution for visualization. Signals were recorded using a MultiClamp 700 A amplifier (Molecular Devices), filtered with a low-pass Bessel filter (4 kHz) and sampled at 20 kHz using PackIO[53]. In target cells with extremely low firing rates the effectiveness of the activity clamp can drop (Supplementary Fig. 2k). Recordings were aborted when the baseline firing rate of the target cell went >4 Hz during the experiment (two cells in two animals). Trials in which the patched cells showed signs of a significant decline in health (that is, the baseline spike rates and/or

amplitudes decreased by >80%, and/or the spike widths, measured as the full width at half maximum, increased by >80% during the recording) were not included in the analysis.

Offline data analysis. Data were analyzed using toolboxes and custom scripts written in MATLAB and Python. PackIO[53] recordings made during all the experiments enabled precise post hoc synchronization of stimulus delivery times and individual imaging frame times. Motion correction was performed on calcium imaging movies using a discrete Fourier transform–based algorithm[50]. Neuropil-subtracted fluorescence traces were extracted using the Suite2P package[54]. We defined GCaMP6s events based on fluorescence traces using a template-matching algorithm[55] (Supplementary Fig. 5). For GCaMP6f, we calculated the inferred spike rate (Fig. 2j,l–m and Supplementary Fig. 12), which is defined as the time average of the spike train (analog) returned by Suite2P[54], and is given in arbitrary units. As an alternative measure of activity in GCaMP6f traces, we defined GCaMP6f events using an iterative routine, in which the event times were adjusted iteratively to obtain the onsets and amplitudes of bursting events (Supplementary Fig. 8). The event onset times were first initialized as the time when the inferred spike amplitude from Suite2P was greater than the mean plus one s.d. Then, in one iteration, the events were discarded if they occurred within a 150 ms window after the preceding event and/or if the amplitude (90% reference level) of the fluorescence signal (measured in a 2 s window around the detected event time, normalized to the average value in 20 frames before the event onset frame) was below zero. The calculated onset times (10% rise time) were adjusted to be the new event onset times, and the iterative procedure was repeated three times (Supplementary Fig. 8b). Event rates are given in Hertz and event amplitudes in $\Delta F/F$ (Supplementary Fig. 9). Neuropil-subtracted calcium traces were smoothed by a low-pass filter (1.5 Hz) and then normalized to the average of the 3% of data points with the lowest calcium fluorescence values before calculating the Pearson's correlation coefficients. For plasticity experiments, the normalized calcium transients were high-pass filtered above 0.02 Hz to correct for slow drifts in baseline in the longer recordings before calculating correlation and population coupling factors[56]. Figure 2i–m includes only experiments in which >100 trigger-target pairings were performed.

Data presentation and statistical analyses. All values are given as mean ± s.d. unless otherwise noted. Statistical analyses were performed using different tests as appropriate, as stated in the figure legends.

Reporting Summary. Further information on research design is available in the Nature Research Reporting Summary linked to this article.

Data availability

The original code, together with detailed instructions, is available at the following Github link: https://github.com/alloptical/ClosedLoop. The authors will keep the repository operating and freely accessible. The data sets generated and/or analyzed in this study are available from the corresponding authors upon reasonable request.

References

26. Chen, T. W. et al. *Nature* **499**, 295–300 (2013).
27. Nikolenko, V., Poskanzer, K. E. & Yuste, R. *Nat. Methods* **4**, 943–950 (2007).
28. Nikolenko, V. et al. *Front. Neural Circuits* **2**, 5 (2008).
29. Guo, Z. V., Hart, A. C. & Ramanathan, S. *Nat. Methods* **6**, 891–896 (2009).
30. Dal Maschio, M. et al. *Opt. Express* **18**, 18720–18731 (2010).
31. Anselmi, F., Ventalon, C., Bègue, A., Ogden, D. & Emiliani, V. *Proc. Natl Acad. Sci. USA* **108**, 19504–19509 (2011).
32. Prakash, R. et al. *Nat. Methods* **9**, 1171–1179 (2012).
33. Packer, A. M. et al. *Nat. Methods* **9**, 1202–1205 (2012).
34. Akerboom, J. et al. *Front. Mol. Neurosci.* **6**, 2 (2013).
35. Hochbaum, D. R. et al. *Nat. Methods* **11**, 825–833 (2014).
36. Theis, L. et al. *Neuron* **90**, 471–482 (2016).
37. Ronzitti, E. et al. *J. Neurosci.* **37**, 10679–10689 (2017).
38. Rickgauer, J. P. & Tank, D. W. *Proc. Natl Acad. Sci. USA* **106**, 15025–15030 (2009).
39. Gerchberg, R. W. & Saxton, W. O. *Optik (Stuttg.)* **35**, 237–246 (1972).
40. Oron, D., Tal, E. & Silberberg, Y. *Opt. Express* **13**, 1468–1476 (2005).
41. Zhu, G., van Howe, J., Durst, M., Zipfel, W. & Xu, C. *Opt. Express* **13**, 2153–2159 (2005).
42. Papagiakoumou, E., de Sars, V., Oron, D. & Emiliani, V. *Opt. Express* **16**, 22039–22047 (2008).
43. Papagiakoumou, E., de Sars, V., Emiliani, V. & Oron, D. *Opt. Express* **17**, 5391–5401 (2009).
44. Papagiakoumou, E. et al. *Nat. Methods* **7**, 848–854 (2010).
45. Andrasfalvy, B. K., Zemelman, B. V., Tang, J. & Vaziri, A. *Proc. Natl Acad. Sci. USA* **107**, 11981–11986 (2010).
46. Hernandez, O. et al. *Nat. Commun.* **7**, 11928 (2016).
47. Pégard, N. C. et al. *Nat. Commun.* **8**, 1228 (2017).
48. Baker, C. A., Elyada, Y. M., Parra, A. & Bolton, M. M. *eLife* **5**, e14193 (2016).
49. Shemesh, O. A. et al. *Nat. Neurosci.* **20**, 1796–1806 (2017).
50. Guizar-Sicairos, M., Thurman, S. T. & Fienup, J. R. *Opt. Lett.* **33**, 156–158 (2008).
51. Kitamura, K., Judkewitz, B., Kano, M., Denk, W. & Häusser, M. *Nat. Methods* **5**, 61–67 (2008).
52. Margrie, T. W. et al. *Neuron* **39**, 911–918 (2003).
53. Watson, B.O., Yuste, R. & Packer, A.M. *bioRxiv* Preprint at https://www.biorxiv.org/content/early/2016/05/18/054080 (2016).
54. Pachitariu, M. *et al. bioRxiv* Preprint at https://www.biorxiv.org/content/early/2017/07/20/061507 (2016).
55. Clements, J. D. & Bekkers, J. M. *Biophys. J.* **73**, 220–229 (1997).
56. Okun, M. et al. *Nature* **521**, 511–515 (2015).

nature research

Corresponding author(s): Michael Hausser

Reporting Summary

Nature Research wishes to improve the reproducibility of the work that we publish. This form provides structure for consistency and transparency in reporting. For further information on Nature Research policies, see Authors & Referees and the Editorial Policy Checklist.

Statistical parameters

When statistical analyses are reported, confirm that the following items are present in the relevant location (e.g. figure legend, table legend, main text, or Methods section).

n/a	Confirmed	
☐	☒	The exact sample size (*n*) for each experimental group/condition, given as a discrete number and unit of measurement
☐	☒	An indication of whether measurements were taken from distinct samples or whether the same sample was measured repeatedly
☐	☒	The statistical test(s) used AND whether they are one- or two-sided *Only common tests should be described solely by name; describe more complex techniques in the Methods section.*
☐	☒	A description of all covariates tested
☐	☒	A description of any assumptions or corrections, such as tests of normality and adjustment for multiple comparisons
☐	☒	A full description of the statistics including central tendency (e.g. means) or other basic estimates (e.g. regression coefficient) AND variation (e.g. standard deviation) or associated estimates of uncertainty (e.g. confidence intervals)
☐	☒	For null hypothesis testing, the test statistic (e.g. *F*, *t*, *r*) with confidence intervals, effect sizes, degrees of freedom and *P* value noted *Give P values as exact values whenever suitable.*
☒	☐	For Bayesian analysis, information on the choice of priors and Markov chain Monte Carlo settings
☒	☐	For hierarchical and complex designs, identification of the appropriate level for tests and full reporting of outcomes
☐	☒	Estimates of effect sizes (e.g. Cohen's *d*, Pearson's *r*), indicating how they were calculated
☐	☒	Clearly defined error bars *State explicitly what error bars represent (e.g. SD, SE, CI)*

Our web collection on statistics for biologists may be useful.

Software and code

Policy information about availability of computer code

Data collection	A custom software package, RTAOI (Real-Time All-Optical Interface), developed using VB.NET Framework 4.5, Visual studio 2013 (Microsoft), CUDA toolkit 8 (NVIDIA), NI-DAQmx 15.5 (National Instruments), together with PrairieLink (Bruker Corporation) and Prairie View 5.4 (Bruker Corporation) was used for microscope control and imaging data collection. Blink SDK (Meadowlark Optics) was used for spatial light modulator control. PackIO (Watson et al, bioRxiv, 2016) was used for read/write electrical signals from National Instruments devices.
Data analysis	The custom software package (RTAOI, as mentioned above) was used for online data analysis; MATLAB2016a and Python 3.5 were used for off-line data analysis; Suite2P (Pachitariu et al, bioRxiv, 2016) was used for off-line analysis of calcium imaging data.

For manuscripts utilizing custom algorithms or software that are central to the research but not yet described in published literature, software must be made available to editors/reviewers upon request. We strongly encourage code deposition in a community repository (e.g. GitHub). See the Nature Research guidelines for submitting code & software for further information.

Data

Policy information about availability of data

All manuscripts must include a data availability statement. This statement should provide the following information, where applicable:

- Accession codes, unique identifiers, or web links for publicly available datasets
- A list of figures that have associated raw data
- A description of any restrictions on data availability

The original code, together with detailed instructions and demo data is available at the following Github link: https://github.com/alloptical/ClosedLoop; Correspondence and requests for raw data should be addressed to M.H. (m.hausser@ucl.ac.uk).

Field-specific reporting

Please select the best fit for your research. If you are not sure, read the appropriate sections before making your selection.

☒ Life sciences ☐ Behavioural & social sciences ☐ Ecological, evolutionary & environmental sciences

For a reference copy of the document with all sections, see nature.com/authors/policies/ReportingSummary-flat.pdf

Life sciences study design

All studies must disclose on these points even when the disclosure is negative.

Sample size	No sample-size calculation was performed. In cases where statistics are reported, we used the minimum number of animals possible to obtain a reasonable estimate of the effect as per the "3R" guidelines required by law in the UK. See the first paragraph of the methods section.
Data exclusions	No samples were excluded except in obvious cases where experiments could no longer be performed due to poor viral expression or occluded chronic windows. In the activity clamp experiments, recordings were aborted and were not included in analysis when the baseline firing rate of the target cell went above 4 Hz. Trials in which the baseline spike rates and/or amplitudes decreased by more than 80%, and/or the spike widths (measured as the full width at half maximum) increased by more than 80% compared to those in the initial recording were not included in analysis(see Methods). Fig. 2i-l only includes experiments in which greater than 100 trigger-targets pairings were performed during conditioning on animals younger than 14 weeks old.
Replication	The reported statistics were based on sufficient sample size; number of replications are stated in the figure legends; experiments were done in batches rather than all at once. The range of the factors that could potentially limit the reproducibility of the experimental results (e.g. animal age, cell spontaneous rate) is provided (see Methods). Multiple ways of analysis were done on the same dataset to show that results were immune to analysis particularities (e.g. both inferred spike rate and calcium event rate were tested to show the change in the activity level in the conditioning experiments in Fig. 2m and Supplementary Fig.8); The exact details of the methods are provided in the methods section.
Randomization	No randomization was necessary since no experimental groups were formed.
Blinding	No blinding was necessary since no group allocation was performed.

Reporting for specific materials, systems and methods

Materials & experimental systems

n/a	Involved in the study
☒	☐ Unique biological materials
☒	☐ Antibodies
☒	☐ Eukaryotic cell lines
☒	☐ Palaeontology
☐	☒ Animals and other organisms
☒	☐ Human research participants

Methods

n/a	Involved in the study
☒	☐ ChIP-seq
☒	☐ Flow cytometry
☒	☐ MRI-based neuroimaging

Animals and other organisms

Policy information about studies involving animals; ARRIVE guidelines recommended for reporting animal research

Laboratory animals	Female wild-type adult mice, approximately 4 weeks to 8 weeks old were used in this study.
Wild animals	No wild animals were used.
Field-collected samples	No field-collected samples were used